

Optical femtosecond filaments in condensed media

S. Skupin, R. Nuter, and L. Bergé

Département de Physique Théorique et Appliquée, CEA-DAM/Île de France, Boîte Postale 12, 91680 Bruyères-le-Châtel, France

(Received 23 February 2006; published 18 October 2006)

The self-guiding of femtosecond light pulses in dense materials is investigated both theoretically and numerically for various laser wavelengths. Special attention is paid on chromatic dispersion, plasma gain, and multiphoton absorption in the nonlinear evolution of ultrashort filaments. First, by mapping the dispersion versus the ratio of beam power over the critical power for self-focusing we justify the existence of special propagation regimes, in which the beam self-channels with weak plasma response. Second, we prove that at low wavelengths multiphoton losses can quench the emission of free electrons, which justifies recent experimental observations of no apparent electron emission in water.

DOI: [10.1103/PhysRevA.74.043813](https://doi.org/10.1103/PhysRevA.74.043813)

PACS number(s): 42.65.-k, 42.68.Ay, 52.38.Hb

I. INTRODUCTION

In the last decade, investigations on laser-produced femtosecond (fs) filaments in gases, liquids, and dielectrics have been raising considerable interest due to their potential applications in remote sensing and pulse compression techniques [1–5]. The long-distance evolution of infrared pulses in gases is nowadays well understood [1]: Optical filaments develop from the dynamic balance between Kerr focusing and plasma defocusing, with a limited influence of chromatic dispersion. This scenario, however, becomes more questionable for dense media [2–5]. Recent works [4,5] reported filamentation regimes mainly driven by nonlinear losses and strong dispersion with minor action of ionization in water experiments. By self-focusing, the beam exhibits an X shape in space and time, resulting from the interplay between diffraction, normal group-velocity dispersion (NGVD), and minimization of energy losses caused by multiphoton absorption (MPA). This dynamics was numerically reproduced in Ref. [6] from a unidirectional paraxial propagation equation describing the full wave dispersion. NGVD was claimed to arrest the wave collapse, with no crucial role played by the plasma nonlinearities. Besides, new propagation regimes involving anomalous group-velocity dispersion (AGVD) were recently studied from the experimental side in Ref. [7] and numerically restored in Ref. [8]. They revealed the possibility of shrinking the pulse both in space and time and to keep it guided over several diffraction lengths. AGVD opens new trends in pulse compression techniques and thus deserves a thorough examination.

The purpose of this work is to discriminate between the respective roles of dispersion, plasma, and multiphoton losses in the generic dynamics of femtosecond pulse propagation. This goal is motivated by the following. First, models exploited in Refs. [4,5] accounted for nonlinear losses, but they discarded plasma sources. Second, NGVD is known to arrest Kerr focusing [9–15] in precise regions delimited by the dispersion lengths and the pulse peak power [11,12], but we still ignore how these regions are modified in the presence of higher-order dispersion and pulse-steepening effects. Here, we solve this issue by numerically mapping the dispersion versus self-focusing from a complete propagation model applied to both NGVD and AGVD regimes. Furthermore we

show that, for low wavelengths, losses caused by multiphoton absorption dominate over plasma defocusing in the self-guiding process. This assessment is supported by theoretical arguments.

To start with, we recall the propagation equations in their “classical” form (see, e.g., Refs. [8,16]), coupling the electric-field envelope \mathcal{E} with the electron plasma density ρ ,

$$\partial_z \mathcal{E} = \frac{i}{2k_0} T^{-1} \nabla_{\perp}^2 \mathcal{E} + i \mathcal{D} \mathcal{E} - i \frac{k_0}{2n_0^2 \rho_c} T^{-1} \rho \mathcal{E} - \frac{\sigma}{2} \rho \mathcal{E} - \frac{U_i W(I) \rho_{nt}}{2I} \mathcal{E} + i \frac{\omega_0}{c} n_2 T \int \mathcal{R}(t-t') |\mathcal{E}(t')|^2 dt' \mathcal{E}, \quad (1)$$

$$\partial_t \rho = W(I) \rho_{nt} + \sigma \rho I / U_i - f(\rho). \quad (2)$$

Here, $I = |\mathcal{E}|^2$, $\nabla_{\perp}^2 = r^{-1} \partial_r r \partial_r$, $k_0 = n_0 \omega_0 / c$, $T = 1 + (i/\omega_0) \partial_t$, \mathcal{D} is the complex-valued dispersion operator treated in Fourier domain and involves linear losses [$\text{Im}\{\tilde{\mathcal{D}}(\omega)\} \neq 0$], $\rho_c (\text{cm}^{-3}) \simeq 1.11 \times 10^{21} / \lambda_0^2 (\mu\text{m})$ is the critical plasma density at the laser wavelength λ_0 , σ is the inverse bremsstrahlung cross section, and n_2 is the nonlinear index for the Kerr response. This may include a Raman-delayed component as

$$\mathcal{R}(t) = (1 - x_{dk}) \delta(t) + x_{dk} [(1 + \Omega^2 \tau_K^2) / \Omega \tau_K^2] \theta(t) e^{-t/\tau_K} \sin(\Omega t)$$

with δ, θ being the Dirac and Heaviside distributions. Two propagation materials will be investigated, namely, silica [8], for which $x_{dk} = 0.18$, $\Omega \tau_K = 2.6$, $\tau_K = 32$ fs [17], and water [6] for which $x_{dk} = 0$. Despite differences in their Kerr responses, these two media promote similar features in the nonlinear dynamics of ultrashort pulses. In Eq. (2), $W(I)$ is the Keldysh ionization rate for crystals [18] with gap potential U_i and ρ_{nt} is the density of neutral atoms. $W(I)$ describes both regimes of tunnel and multiphoton ionization (MPI). In the MPI limit, $W(I)$ can be simplified as $\sigma_K I^K$, where σ_K is the ionization cross section and $K \equiv \langle (U_i / \hbar \omega_0) + 1 \rangle$ is the number of photons necessary to promote one electron in the conduction band. Avalanche ionization characterized by the parameter σ is also included. Electron-ion recombination intervenes through the function $f(\rho) = \rho / \tau_r$ with $\tau_r = 150$ fs in silica [16] and $f(\rho) = a \rho^2$ with $a = 2 \times 10^{-24} \text{ cm}^3/\text{fs}$ in water [6].

This model also includes space-time focusing and self-steepening through the operators T, T^{-1} , as established in

Refs. [16,19]. It, however, discards nonlinear optical saturation induced by, e.g., $\chi^{(5)}$ defocusing susceptibility [20], together with vectorial and nonparaxial effects [21]. On the one hand, $\chi^{(5)}$ corrections are nowadays not available for the materials and wavelengths considered here. Despite this, it can be shown that the ratio between the fifth and third-order nonlinear polarization, $|P^{(5)}/P^{(3)}| \approx |E/E_{at}|^2$, where E is the laser field and $E_{at} \approx 3 \times 10^8$ V/cm [22], remains smaller than 0.4 for laser intensities lower than 5×10^{13} W/cm². On the other hand, vectorial as well as nonparaxial contributions are negligible as long as the transverse size of the beam remains large compared with the laser wavelength, which will always be satisfied throughout the coming analysis.

Pulses are assumed to be initially Gaussian,

$$\mathcal{E}(r, t, z = 0) = \sqrt{\frac{2P_{in}}{\pi w_0^2}} e^{-(r^2/w_0^2) - (t^2/t_p^2) - ik_0 r^2/2f}, \quad (3)$$

where P_{in} , w_0 , t_p , and f denote their input peak power, waist, duration, and focal length, respectively.

Preliminary computations (not shown here) enabled us to recover the nonlinear dynamics of Ref. [6] for propagation in water at $\lambda_0 = 527$ nm. With Eqs. (1) and (2), 100 μ m waisted, 170 fs Gaussian pulses focused with $f = 5$ cm were simulated for 1.3–2.6 μ J energies, corresponding to beam powers ranging from 5 to 10 critical powers for self-focusing ($P_{cr} \approx \lambda_0^2/2\pi n_0 n_2$). Using the same material parameters, we faithfully reproduced the spectral intensity, multi-peaked temporal distortions, and maximum fluences formerly published in Ref. [6]. Moreover, by imposing the limits $T, T^{-1} \rightarrow 1$, we refound quite close results. This property was found to hold also in fused silica samples: Although higher-order dispersion and pulse steepening substantially enlarge spectral blue-shifts and asymmetricize temporal distributions, they cannot be responsible—at least for the pulse durations selected ($t_p \geq 10$ fs)—for either arresting the beam collapse, or supporting the self-guiding dynamics by themselves. So, the key players for pulse propagation appear to be definitively self-focusing, GVD, plasma gain, and losses. Among the free-electron sources of Eq. (2), avalanche was checked to poorly contribute to the overall electron density. Plasma is then mainly originating from the photoionization source $W(I)$.

In what follows, we discriminate the previous effects separately. To this aim, we shall employ a dimensionless model derived from Eqs. (1) and (2) in the limit $x_{dk} \rightarrow 0$, using the substitutions $z \rightarrow 4z_0 z$, $t \rightarrow tt_p$, $\mathcal{E} \rightarrow \sqrt{P_{cr}/4\pi w_0^2} \psi$, $\rho \rightarrow (n_0^2 \rho_c / 2z_0 k_0) \rho$, with $z_0 = n_0 \pi w_0^2 / \lambda_0$, which yields the extended nonlinear Schrödinger (NLS) equation [26]

$$i\partial_z \psi + \nabla_{\perp}^2 \psi + |\psi|^2 \psi + \mathcal{F}(\psi) = 0. \quad (4)$$

In Eq. (4), $\mathcal{F}(\psi) = -\delta \partial_t^2 \psi - \rho \psi + i\nu |\psi|^{2K-2} \psi$ only involves leading-order contributions from GVD with coefficient $\delta \equiv 2z_0 k'' / t_p^2$, where $k'' = \partial_{\omega}^2 k|_{\omega=\omega_0}$, plasma response in the MPI limit $\partial_t \rho = \Gamma |\psi|^{2K}$ with $\Gamma = (2z_0 k_0 / n_0^2 \rho_c) \sigma_K \rho_{ni} t_p (P_{cr} / 4\pi w_0^2)^K$, and MPA with $\nu = 2z_0 U_i \sigma_K \rho_{ni} (P_{cr} / 4\pi w_0^2)^{K-1}$.

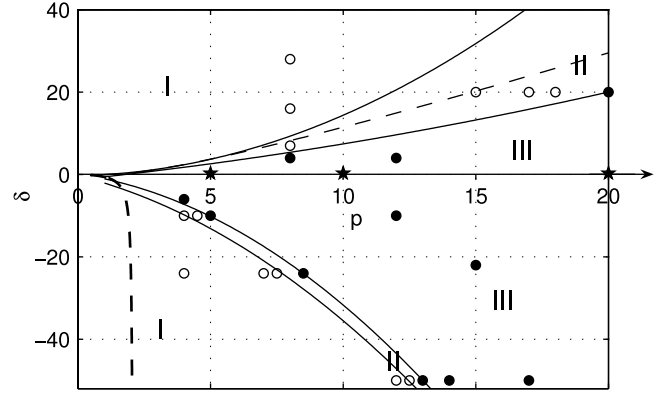


FIG. 1. Collapse regions in the plane (δ, p) . The solid curves extrapolate results from numerical integrations of Eqs. (1) and (2). The dashed curves represent theoretical limits estimated from Eq. (4), above which dispersion inhibits self-focusing.

II. CHROMATIC DISPERSION

Let us first discuss the effect of dispersion, for which $\mathcal{F} = -\delta \partial_t^2 \psi$ in Eq. (4). Pioneering analyses [9–11] evidenced that NGVD ($k'' > 0$) is capable of arresting the beam collapse by splitting a self-focusing pulse into symmetric peaks in the time domain. This property is currently recovered in numerical computations involving input powers moderately above critical. However, knowing whether dispersion completely halts the collapse by pulse splitting at very high powers remains an open issue (see, e.g., Refs. [14,15]), as the field amplitude sharply increases by several decades. In the present context, however, these peak growths are expected to be saturated by other nonlinear phenomena, such as plasma generation. For purely dispersive media, Chernev and Petrov [11] and Luther *et al.* [12] proved that NGVD prevents self-focusing in some ranges of power ratios $p = P_{in}/P_{cr}$ as long as the normalized dispersion length $t_p^2/2z_0 k''$ is small enough, i.e., $\delta > \delta_{crit}(p)$. The power-dependent bound δ_{crit} , derived for example, in Ref. [12], has been recalled in the upper half plane of Fig. 1 ($\delta > 0$) by a dashed line. It signifies that at high enough powers [$\delta < \delta_{crit}(p)$], GVD cannot efficiently compete with Kerr focusing, which still promotes a violent growth of the optical field. In this configuration, self-focusing is saturated by plasma generation. The lower solid curve represents the same boundary inferred from numerous simulations involving all physical ingredients of Eqs. (1) and (2) for negligible linear losses. Open circles represent some initial conditions that do not collapse for silica parameters; closed ones refer to those yielding plasma saturation, for which the peak intensity can reach its maximum value, henceforth noted I_{pl} . Black stars specify the collapsing states emerging from water data. They indicate arrest of collapse through the nonlinear losses, as will be discussed in the next section.

By “collapse,” we mean self-focused states that reach diverging intensity values and follow the route of a singular, blowing-up solution [13,23]. Only through this singular dynamics, high enough intensity levels, capable of triggering a significant generation of plasma, can be attained. Therefore, three zones can be deduced from Fig. 1.

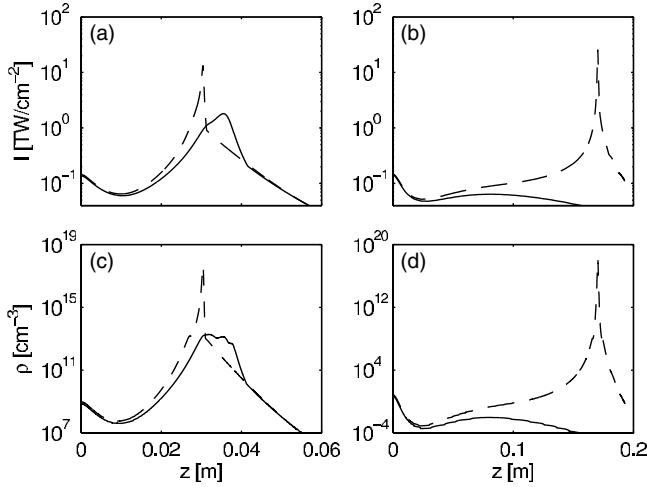


FIG. 2. Peak intensities for Gaussian pulses in fused silica with (a) $p=17$ (solid curve) and $p=18$ (dashed curve) at 790 nm for $\delta=20$ ($w_0=130 \mu\text{m}$; $t_p=19$ fs); (b) $p=12.5$ (solid curve) and $p=13$ (dashed curve) at 1550 nm for $\delta=-50$ ($w_0=260 \mu\text{m}$; $t_p=15$ fs). (c) and (d) show their corresponding electron densities.

(I) A dispersion-dominated domain leading to pure spreading.

(II) A transient zone in which GVD rapidly inhibits the self-focusing by pulse splitting. Although the beam intensity may increase to some extent, it remains smaller than I_{pl} . The plasma response is then limited to small amplitudes and has a minor incidence on the self-guiding.

(III) A Kerr-dominated region, in which chromatic dispersion is unable to stop the collapse before significant plasma generation comes into play.

An equivalent mapping can be done for AGVD regimes ($\delta < 0$): As long as the total (r, t) -gradient norm of the input pulse remains below that of the 3D NLS ground state [8,25], no blowup occurs from Eq. (4). The corresponding frontier, $|\delta| > \delta_{\text{crit}}(p)$, is plotted as a dashed line in the lower half plane of Fig. 1. Again, numerical integrations of the complete Eqs. (1) and (2) shift the zones of no blowup to some extent, displayed by the solid curves. Differences with boundaries fixed by the NLS equation (4) are caused by higher-order dispersion and self-steepening that break the symmetry of the temporal pulse profile. This prevents the beam energy from being fully engaged in the collapse process and “delays” it noticeably. It is worth noting that, because conditions for beam collapse become sharper with anomalous GVD and overcome the basic requirement of a critical power, self-focusing can here still develop for $p < 1$ in various focusing geometries, when, e.g., a convergent lens is introduced along the optical path.

Region II in Fig. 1 emphasizes the possibility to select appropriate pulse parameters to keep the plasma response at moderate levels. As an example, Figs. 2(a) and 2(c) compare peak intensities and peak electron densities of Gaussian pulses conveying high powers in fused silica at 790 nm ($k'' \approx 370 \text{ fs}^2/\text{cm}$) with the NGVD parameter $\delta=20$. For $p > p_{\text{lim}}=17$, plasma occurs, as the wave intensity grows up to two decades above the initial wave intensity ($>15 \text{ TW}/\text{cm}^2$). In contrast, with $p \leq p_{\text{lim}}$, plasma density is

small but nonzero. Figures 2(b) and 2(d) provide similar information for pulses propagating in the AGVD regime at $\lambda_0=1550 \text{ nm}$ ($k''=-280 \text{ fs}^2/\text{cm}$) when $\delta=-50$ and $p=12.5$ or 13. For very high values of $|\delta|$, dispersion prevails over transverse diffraction. It blocks free-electron emission and related losses by inhibiting the collapse process even for powers as high as $p=12.5$. When p is increased, Kerr-focusing and plasma-defocusing cycles produce narrow collapse events associated with intensity levels $>25 \text{ TW}/\text{cm}^2$ and peak electron densities $>10^{17} \text{ cm}^{-3}$. Note that, with a narrower zone II, transitions between spreading and collapsing regimes are sharper than for normal dispersion: Whereas the latter arrests the collapse by splitting the pulse at lower intensity values, anomalous dispersion, instead, favors compression in time.

The dynamics of region II are new. They refer to strongly dispersive regions that maintain the beam in a waveguided shape (i.e., within a slowly diffracting regime) at relatively high powers. They, however, do not apply to the pulse parameters selected in Refs. [4–6] for water propagation. Here, even with a high NGVD coefficient ($k'' \sim 500 \text{ fs}^2/\text{cm}$), the laser parameters ($t_p=170$ fs, $w_0 \sim 100 \mu\text{m}$, $p=5-10$) make the initial pulse always belong to the region III, where chromatic dispersion cannot stop self-focusing and plasma generation (see the black stars in Fig. 1). This statement thus sounds in contradiction with the major conclusion of Refs. [4–6], according to which an apparent absence of free-electron emission characterizes the self-guiding of ultrashort pulses in water cells. To understand the plasma dynamics in this case, it is, therefore, necessary to revisit the respective actions of MPI and MPA carefully.

III. PLASMA RESPONSES: NONLINEAR LOSSES VERSUS FREE-ELECTRON EMISSION

If normal GVD is not efficient enough to arrest the wave collapse, which key player intervenes to avoid an extensive production of free electrons? By “extensive,” we mean that the Kerr and plasma defocusing terms in Eq. (1) mutually compete to produce peak electron densities reaching their maximal value. Assuming $\rho \approx t_p W(I) \rho_{nt}$, we estimate the peak optical intensity attainable in the extensive plasma regime, I_{pl} , by the root of the relation $2n_0 n_2 \rho_c I_{pl} = t_p W(I_{pl}) \rho_{nt}$. $W(I)$ has been plotted in the inset of Fig. 3. We have numerical evidence that among all competitors able to arrest the wave collapse in the region III of Fig. 1, only MPA can lower the peak optical intensity below I_{pl} . So, it seems logical to concentrate on MPA [$\sim W(I)\mathcal{E}/I$] and plasma defocusing [$\sim i\rho\mathcal{E}/\rho_c$] only. Plasma defocusing works by acting on the field phase, whereas MPA is a loss term. Although these two quantities are intimately linked, their respective weights are dictated by the intensity ratio I^*/I , with $I^* \equiv n_0^2 \rho_c U_i / k_0 t_p \sim 1/\lambda_0 t_p$. By setting $I=I_{pl}$, the intensity ratio I^*/I_{pl} yields an estimate of the MPA efficiency close to plasma saturation for different wavelengths. The resulting curve has been represented in Fig. 3 for fused silica, water, and air at various pulse durations. It shows that the percentage of MPA over the emission of free electrons (plasma gain) augments all the more as the laser wavelength is low and the pulse duration is

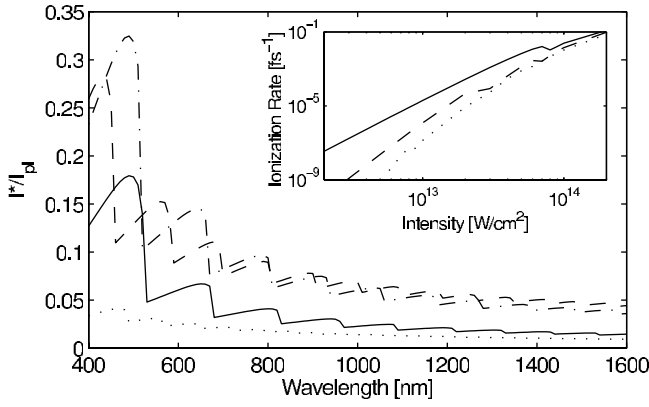


FIG. 3. I^*/I_{pl} vs λ_0 for different durations t_p in air (70 fs, dotted curve), in fused silica (20 fs, dashed curve), and in water (170 fs, solid curve; 50 fs, dash-dotted curve). The inset shows $W(I)$ vs I at 527 nm in water (solid curve), at 790 nm (dashed curve) and 1550 nm (dotted curve) in silica.

short. The dotted line illustrates the same ratio for 70 fs pulse propagation in air (O_2) molecules [1], for which the PPT (Perelomov *et al.*) [24] ionization rate was employed. Here, MPA becomes negligible compared with MPI. On the whole, Fig. 3 shows the ability of the laser wavelength λ_0 to enhance the role of multiphoton losses in dense media.

The crucial role of the laser wavelength can be confirmed by means of a quasi-self-similar analysis based on Eq. (4). It is well known [26,27] that along the collapse stage the pulse self-focuses with a typical radius $R(z,t)$ as $|\psi| \rightarrow \phi(\xi)/R(z,t)$, where $\xi \equiv r/R(z,t)$ and ϕ is the Townes mode [$\phi(0) \approx 2.2$] reached in the limit $R \rightarrow 0$ while $\beta \equiv -\frac{1}{4}R^3 R_{zz} \geq 0$. We can thus construct a dynamical system for β measuring the weights of MPA and plasma defocusing as potential competitors halting the wave collapse. Considering only photoionization players in $\mathcal{F}(\psi)$ yields near the first collapsing time slice ($t=0$),

$$\beta_z \approx C(R) \left\{ -\frac{\nu}{K} + \frac{R_z}{R} \Gamma \sqrt{\frac{\pi K(K-1)\phi^2(0)}{8(K+1)^2}} \right\}, \quad (5)$$

where $R_z < 0$ and $C(R)$ is a positive factor $\sim R^{2-2K}$. This relation shows that the self-focusing process can be arrested ($\beta_z < 0$) by MPA rather than by MPI, whenever the nonlinear compression rate $|R_z/R|$ satisfies in physical units

$$\left| \frac{R_z}{R} \right| < \frac{n_2 I^*}{\lambda_0} \frac{(K+1)^2}{K^{3/2}(K-1)} \frac{\sqrt{32\pi}}{\phi^2(0)}, \quad (6)$$

which is directly related to the laser wavelength ($I^* \sim 1/\lambda_0$, $K \sim \lambda_0$). The compression rate $|R_z/R|$ is linked to the ratio of peak intensity over the initial intensity. It strongly increases near the collapse point and at small enough wavelengths, nonlinear losses can actually be the key player maintaining the beam in a self-channeled state.

To verify the previous property, we performed numerical simulations from Eqs. (1) and (2), using the pulse parameters defined above for water propagation at 527 nm with an input energy of $2.6 \mu\text{J}$ ($p=10$). Figure 4(a) shows the peak intensity when ρ and MPA are both set equal to zero (dashed

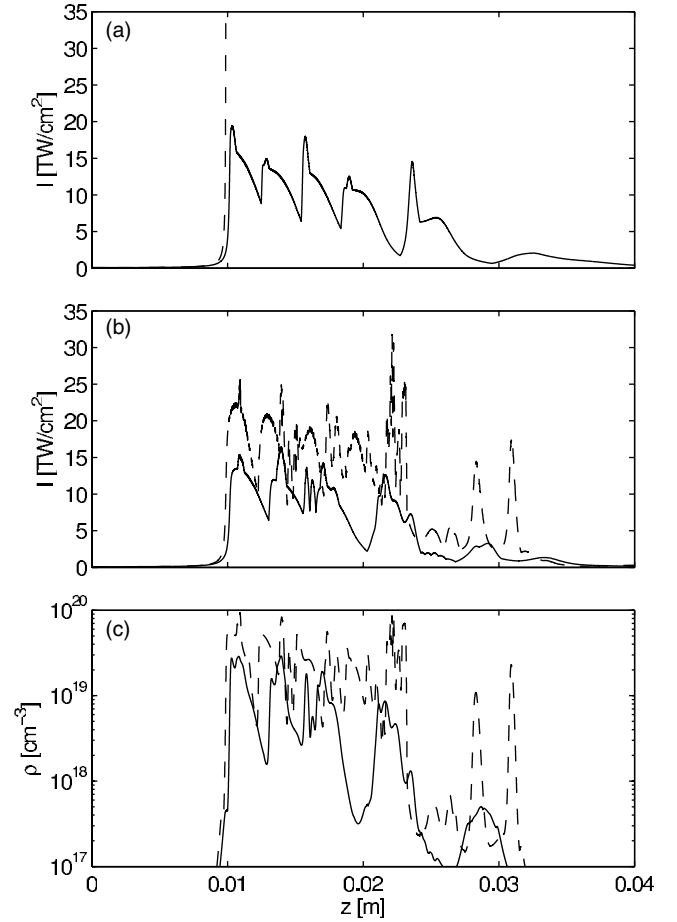


FIG. 4. Peak intensities of 170 fs pulses with $w_0=100 \mu\text{m}$, $f=5 \text{ cm}$ ($p=10$) in water at $\lambda_0=527 \text{ nm}$ for (a) $\rho=\text{MPA}=0$ (dashed curve), with no plasma gain (solid curve), (b) for the full model (1) and (2) (solid curve), and when omitting MPA alone (dashed curve). (c) Peak electron densities corresponding to (b).

curve), and when the plasma defocusing term $\sim i\rho\mathcal{E}/\rho_c$ is omitted (solid curve). Figure 4(b) shows that obtained from the complete model (1) and (2) (solid curve) and when the MPA term is removed (dashed curve). Normal GVD cannot stop Kerr focusing, as expected from Fig. 1. By setting $\tilde{D}(\omega)=0$, we inferred in this respect that the only (but important) action of GVD on the filament evolution is to cut the plasma range by dispersing the pulse time slices. With $\rho=0$, the maximum intensity remains close to that computed from the full model, whereas it departs to noticeably higher values when MPA vanishes. Figure 4(c) details the peak electron densities for the full model equations (solid curve) and when MPA is ignored (dashed curve). In both cases, the (generic) FWHM diameter of the Gaussian-shaped plasma channel was observed to be about $1.5 \mu\text{m}$. The absence of MPA promotes an extensive plasma generation exceeding by at least one decade that taking place with nonlinear losses. We observed similar features for shorter pulses with $t_p=50 \text{ fs}$. This property was moreover checked to hold at higher powers ($p=20$).

Figure 5 details the on-axis temporal dynamics of the former pulses in the plane (z,t) . It shows focusing and defocusing cycles over a guiding range of 3 cm, with normal

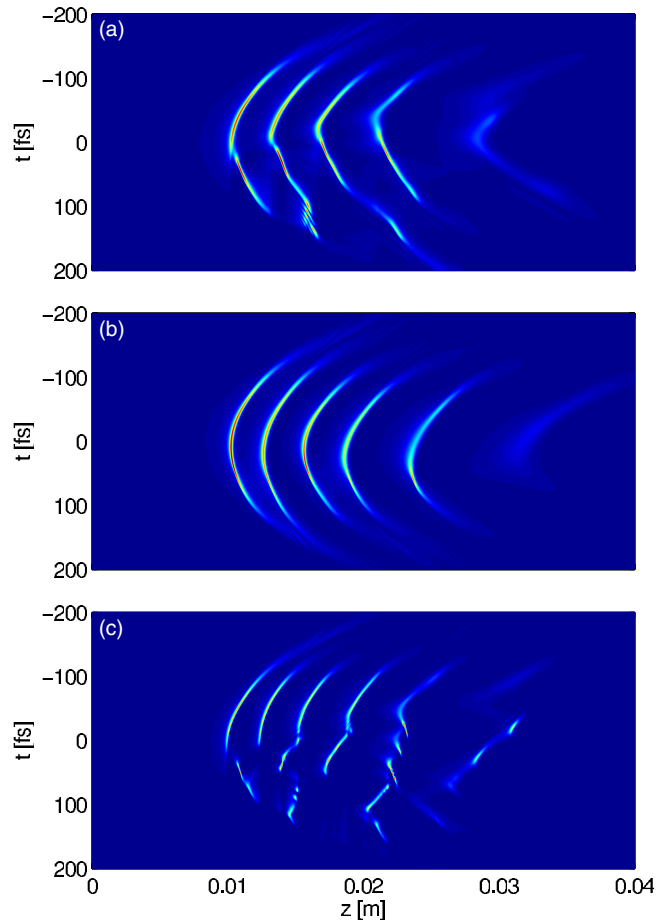


FIG. 5. (Color online) On-axis temporal dynamics vs z of 170 fs pulses with $w_0=100 \mu\text{m}$, $f=5 \text{ cm}$ ($p=10$) in water at $\lambda_0=527 \text{ nm}$ for (a) the full model (1) and (2), (b) for $\rho=0$, and (c) for omitting MPA alone.

GVD dispersing the pulse along each cycle. It is seen right away that the dynamics without plasma gain [Fig. 5(b)] is very close to that of the full model [Fig. 5(a)]. In contrast, when MPA is omitted [Fig. 5(c)] the collapse is arrested by extensive plasma generation, which couples back on the field evolution: The defocusing action of the plasma sharply destroys the regular arches at the trailing edge of the pulse. This dynamics signals a relevant action of the free electrons onto the self-guiding.

For comparison, Figs. 6(a) and 6(b) depict the propagation for $\lambda_0=1 \mu\text{m}$ when again $f=5 \text{ cm}$. We clearly see that the modification induced by MPA on the plasma response becomes much smaller as λ_0 is increased. The peak electron densities shown in Fig. 6(a) for the full model (solid line) and when omitting MPA (dashed line) are almost the same. Here, the FWHM diameter of the Gaussian-shaped plasma channel is increased to $\sim 3 \mu\text{m}$ due to the larger wavelength. For the full model, we observe almost the same (mean) peak electron density as at $\lambda_0=527 \text{ nm}$, namely, $\sim 10^{19} \text{ cm}^{-3}$. So, over comparable propagation scales, the amount of free electrons should be four times higher at $1 \mu\text{m}$ than at 527 nm . Furthermore, Fig. 6(b) supplies the temporal evolution of the pulse at $1 \mu\text{m}$ wavelength. By confronting this subplot with Fig. 5, it is obvious that the defocusing action of the plasma

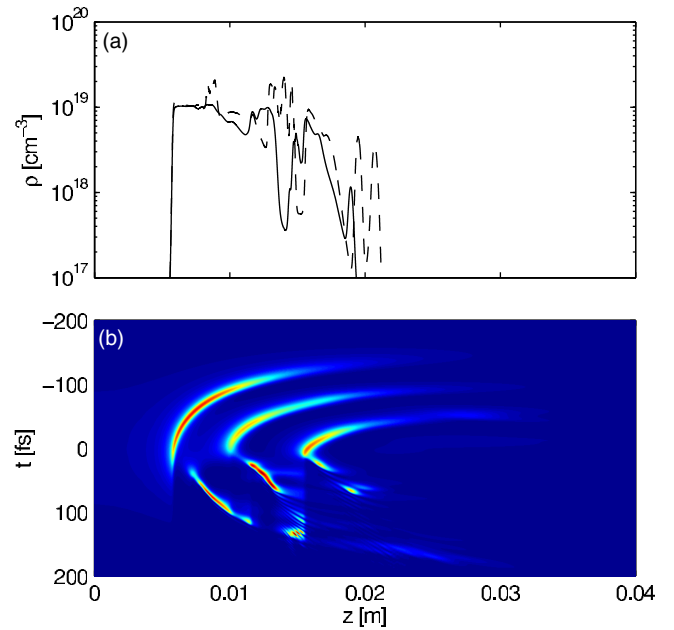


FIG. 6. (Color online) (a) Peak electron densities of 170 fs pulses with $w_0=100 \mu\text{m}$, $f=5 \text{ cm}$ ($p=10$) in water at $\lambda_0=1 \mu\text{m}$ for the full model (1) and (2) (solid curve), and when omitting MPA alone (dashed curve). (b) On-axis temporal distribution vs z for the full model at the same wavelength.

has an important impact on the propagation dynamics. In particular, the trailing edge of the pulse is strongly distorted by the plasma channel generated by its front part.

Finally, to evaluate the incidence of the focusing geometry onto this dynamics, we performed additional runs using the same pulse parameters as in Fig. 4, except that $f=+\infty$.

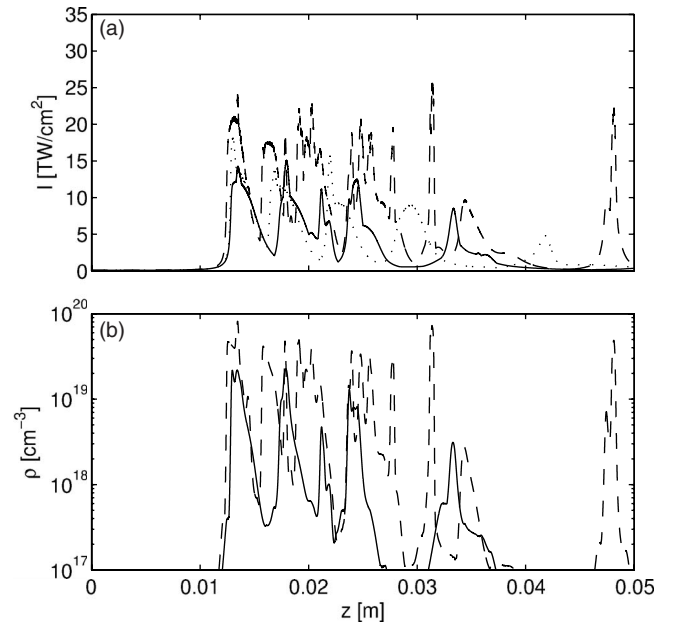


FIG. 7. (a) Peak intensities of 170 fs pulses with $w_0=100 \mu\text{m}$, $f=+\infty$ ($p=10$) in water at $\lambda_0=527 \text{ nm}$ for the full model (1) and (2) (solid curve), with no plasma gain (dotted curve), and when omitting MPA alone (dashed curve). (b) Peak electron densities corresponding to (a).

The results shown in Fig. 7 evidence that the predominance of the nonlinear losses compared with the plasma gain still holds in parallel geometry. Apart from a shift of the nonlinear focus point to slightly larger propagation distances (1.3 cm instead of 1 cm), the results are qualitatively the same as in the loose focusing geometry with $f=5$ cm.

IV. CONCLUSION

In summary, we have cleared up the respective roles of GVD, multiphoton absorption, and plasma defocusing in condensed transparent media traversed by intense, ultrashort laser pulses. Chromatic dispersion may arrest the collapse of high-power pulses provided the normalized GVD length $t_p^2/2z_0k''=1/\delta$ is small enough for a given power ratio P_{in}/P_{cr} . When dispersion cannot saturate Kerr focusing at high power levels, there exists a subtle competition between

the nonlinear absorption and the photoionization source. At low wavelengths, MPA saturates the Kerr compression and stabilizes the beam over long distances. This scenario applies to Dubietis *et al.*'s experiments [4], for which a propagation model mainly relying on nonlinear losses (the so-called NLL model) was proposed. More generally it applies to femtosecond filaments in media with high critical plasma densities ρ_c . Free electron generation still takes place, but the plasma coupling has a weak influence on the propagation dynamics. The beam self-guiding is then mainly supported by nonlinear absorption.

ACKNOWLEDGMENTS

The authors thank Dr. D. Faccio for fruitful discussion and Dr. M. Kolesik for providing us with the water parameters used in Ref. [6].

-
- [1] A. Braun, G. Korn, X. Liu, D. Du, J. Squier, and G. Mourou, *Opt. Lett.* **20**, 73 (1995). See J. Kasparian, M. Rodriguez, G. Méjean, J. Yu, E. Salmon, H. Wille, R. Bourayou, S. Frey, Y. B. André, A. Mysyrowicz, R. Sauerbrey, J. P. Wolf, and L. Wöste, *Science* **301**, 61 (2003) for review.
- [2] S. Tzortzakis, L. Sudrie, M. Franco, B. Prade, A. Mysyrowicz, A. Couairon, and L. Bergé, *Phys. Rev. Lett.* **87**, 213902 (2001); W. Liu, S. L. Chin, O. Kosareva, I. S. Golubtsov, and V. P. Kandidov, *Opt. Commun.* **225**, 193 (2003); J. Liu, H. Schroeder, S. L. Chin, R. Li, and Z. Xu, *Opt. Express* **13**, 10248 (2005).
- [3] A. A. Zozulya, S. A. Diddams, A. G. Van Engen, and T. S. Clement, *Phys. Rev. Lett.* **82**, 1430 (1999); A. L. Gaeta, *ibid.* **84**, 3582 (2000); H. Ward and L. Bergé, *ibid.* **90**, 053901 (2003); V. P. Kandidov, I. S. Golubtsov, and O. G. Kosareva, *Quantum Electron.* **34**, 348 (2004); J. Liu, H. Schroeder, S. L. Chin, R. Li, W. Yu, and Z. Xu, *Phys. Rev. A* **72**, 053817 (2005).
- [4] A. Dubietis, G. Tamošauskas, I. Diomin, and A. Varanavičius, *Opt. Lett.* **28**, 1269 (2003); A. Dubietis, E. Gaižauskas, G. Tamošauskas, and P. Di Trapani, *Phys. Rev. Lett.* **92**, 253903 (2004).
- [5] C. Conti, S. Trillo, P. Di Trapani, G. Valiulis, A. Piskarskas, O. Jedrkiewicz, and J. Trull, *Phys. Rev. Lett.* **90**, 170406 (2003); M. A. Porras, A. Parola, D. Faccio, A. Dubietis, and P. Di Trapani, *ibid.* **93**, 153902 (2004).
- [6] M. Kolesik, E. M. Wright, and J. V. Moloney, *Phys. Rev. Lett.* **92**, 253901 (2004).
- [7] K. D. Moll and A. L. Gaeta, *Opt. Lett.* **29**, 995 (2004).
- [8] L. Bergé and S. Skupin, *Phys. Rev. E* **71**, 065601(R) (2005).
- [9] N. A. Zharova, A. G. Litvak, T. A. Petrova, A. M. Sergeev, and A. D. Yunakovskii, *JETP Lett.* **44**, 13 (1986).
- [10] J. E. Rothenberg, *Opt. Lett.* **17**, 584 (1992).
- [11] P. Chernev and V. Petrov, *Opt. Lett.* **17**, 172 (1992); *Opt. Commun.* **87**, 28 (1992).
- [12] G. G. Luther, J. V. Moloney, A. C. Newell, and E. M. Wright, *Opt. Lett.* **19**, 862 (1994).
- [13] L. Bergé, *Phys. Rep.* **303**, 259 (1998).
- [14] K. Germachewski, R. Grauer, L. Bergé, V. K. Mezentsev, and J. J. Rasmussen, *Physica D* **151**, 175 (2001).
- [15] G. Fibich, W. Ren, and X.-P. Wang, *Phys. Rev. E* **67**, 056603 (2003).
- [16] S. Skupin and L. Bergé, *Physica D* **220**, 14 (2006).
- [17] G. P. Agrawal, *Nonlinear Fiber Optics*, 3rd ed. (Academic Press, San Diego, 2001).
- [18] L. V. Keldysh, *Sov. Phys. JETP* **20**, 1307 (1965).
- [19] Th. Brabec and F. Krausz, *Phys. Rev. Lett.* **78**, 3282 (1997).
- [20] N. Aközbek, C. M. Bowden, A. Talebpour, and S. L. Chin, *Phys. Rev. E* **61**, 4540 (2000); A. Vinçotte and L. Bergé, *Phys. Rev. A* **70**, 061802(R) (2004).
- [21] G. Fibich and B. Ilan, *Physica D* **157**, 112 (2001).
- [22] Y. R. Shen, *The Principles of Nonlinear Optics* (Wiley-Interscience, New York, 1984).
- [23] J. Juul Rasmussen and K. Rypdal, *Phys. Scr.* **33**, 481 (1986).
- [24] A. M. Perelomov, V. S. Popov, and M. V. Terent'ev, *Sov. Phys. JETP* **23**, 924 (1966).
- [25] E. A. Kuznetsov, J. Juul Rasmussen, K. Rypdal, and S. K. Turitsyn, *Physica D* **87**, 273 (1995).
- [26] S. Champeaux and L. Bergé, *Phys. Rev. E* **68**, 066603 (2003).
- [27] G. Fibich and G. Papanicolaou, *SIAM J. Appl. Math.* **60**, 183 (1999).